Available online at www.sciencedirect.com
ScienceDirect
Journal of Power Sources 178 (2008) 26–33
JOURNAL OF POWER SOURCES
www.elsevier.com/locate/jpowsour

Heterogeneous electrolyte ($YSZ–Al_2O_3$) based direct oxidation solid oxide fuel cell

J.S. Thokchom[a], H. Xiao[b], M. Rottmayer[c], T.L. Reitz[c], B. Kumar[a,*]

[a] *University of Dayton Research Institute, Dayton, OH 45469-0170, USA*
[b] *Aerospace Power and Propulsion, UES Corp., Dayton, OH 45432-1894, USA*
[c] *Air Force Research Laboratory, Wright Patterson Air Force Base, OH 45433-7251, USA*

Received 19 October 2007; received in revised form 4 December 2007; accepted 5 December 2007
Available online 14 December 2007

Abstract

Bilayers comprised of dense and porous $YSZ–Al_2O_3$ (20 wt%) composite were tape cast, processed, and then fabricated into working solid oxide fuel cells (SOFCs). The porous part of the bilayer was converted into anode for direct oxidation of fuels by infiltrating CeO_2 and Cu. The cathode side of the bilayer was coated with an interlayer [$YSZ–Al_2O_3$ (20 wt%)]: LSM (1:1) and LSM as cathode. Several button cells were evaluated under hydrogen/air and propane/air atmospheres in intermediate temperature range and their performance data were analyzed. For the first time the feasibility of using $YSZ–Al_2O_3$ material for fabricating working SOFCs with high open circuit voltage (OCV) and power density is demonstrated. AC impedance spectroscopy and scanning electron microscopy (SEM) techniques were used to characterize the membrane and cell.

Keywords: Yttria stabilized zirconia; Alumina; Composite; Tape cast; Membrane; Microstructure; Ionic conductivity; Power density

1. Introduction

Solid oxide fuel cells (SOFCs) are believed to be a critical component of the future power generation technologies due to their high fuel to power conversion efficiency with a minimal adverse influence on the environment. However, significant hurdles remain before they become widely acceptable. These hurdles include operating temperatures, mechanical integrity, thermal instability, and cost. Prior investigations report that a high concentration of Al_2O_3 dopant in yttria stabilized zirconia (YSZ) and scandium stabilized zirconia (ScSZ) is not detrimental, can even enhance the conductivity and thus lower the operating temperature of SOFCs [1,2]. The enhancement in the conductivity was attributed to the formation of space charge regions in the vicinity of $YSZ–Al_2O_3$ boundaries. Mori et al. reported a superior conductivity and an improved mechanical strength of the $YSZ–Al_2O_3$ composite electrolytes [3]. The electrical conductivity measurements on the $YSZ–Al_2O_3$ heterogeneous specimens by Feighery and Irvine [4] also suggested that there is no change in conductivity value after doping YSZ with 10 wt% Al_2O_3. But the conductivity decreased for higher doping levels (>10 wt%). A recent work [5] reports that conductivity of heterogeneous specimens in the $YSZ–Al_2O_3$ system is higher because of increased mobility of oxygen vacancies. Furthermore, use of Al_2O_3 would lower the cost of the SOFCs because the cost of Al_2O_3 is about one tenth of the cost of YSZ. So far the development of SOFCs has been focused mainly on YSZ. Development of composites based on YSZ for SOFC electrolyte and electrode materials would open up new avenues in solving the challenges facing commercialization of SOFCs.

In this paper we report for the first time the feasibility of using $YSZ–Al_2O_3$ material for fabricating working SOFCs in the $Cu–CeO_2/YSZ–Al_2O_3$/LSM anode/electrolyte/cathode configuration with an open circuit voltage (OCV) approaching theoretical limit and a reasonable power density at 700 °C.

2. Experimental procedure

2.1. $YSZ–Al_2O_3$ single and bilayer tape cast processing

A quantity of 8YSZ [(8 mol% yttria doped zirconia), NexTech Materials Ltd., Lewis Center, OH] powder with particle

* Corresponding author. Tel.: +1 937 229 3452; fax: +1 937 229 3433.
E-mail address: kumarb@udri.udayton.edu (B. Kumar).

0378-7753/$ – see front matter © 2007 Elsevier B.V. All rights reserved.
doi:10.1016/j.jpowsour.2007.12.009

Table 1
Tape cast (dense and porous layer) batch formulations for YSZ–Al_2O_3 bilayer membrane

Ingredients	YSZ–Al_2O_3 (20 wt%) dense layer batch		[YSZ–Al_2O_3 (20 wt%)]-graphite porous layer batch	
	Wt%	Weight (g)	Wt%	Weight (g)
Part I: milling for 24 h				
YSZ–Al_2O_3 (20 wt%) powder	61.95	40.27	34.07	20.44
Graphite 300 mesh	–	–	27.88	16.73
Menhaden fish oil	1.24	0.81	1.24	0.74
Xylene	15.31	9.95	15.31	9.19
Alcohol	15.31	9.95	15.31	9.19
Part II: milling for another 24 h				
Butylbenzyl phthalate (plasticizer I)	1.55	1.01	1.55	0.93
Poly akylene glycol (plasticizer II)	1.55	1.01	1.55	0.93
Polyvinyl butyal (binder)	3.09	2.01	3.09	1.85
Total	100.00	65.01	100.00	60.00

size of 250 nm was mixed with alumina (Al_2O_3) nanopowder (Nanotek®, Bur Ridge, IL) and subsequently mechanically milled for 0.5 h. The milled batch was mixed with Menhaden fish oil (Blown Z-3), xylene, and alcohol in a glass jar. The glass jar with the batch was tumbled for 24 h. A binder (polyvinyl butyral, B-98) and a mixture of plasticizers [butylbenzyl phthalate, S-160, and poly(alkaline) glycol)] were subsequently introduced and the mixture was tumbled for another 24 h. A similar batch using homogeneously milled YSZ–Al_2O_3 and 28 wt% of graphite fine powder (Aldrich, Milwaukee, WI) as pore former was also prepared in a separate jar. Typical tape cast batches for the dense and porous tapes are presented in Table 1. The resulting slurry without the pore former was cast onto a Mylar® (Dupont, Wilmington, DE) sheet using a clean and firm doctor blade, hereafter termed as dense layer. After 2 h, the second slurry containing the graphite powder as pore former was cast over the dense layer, hereafter named as porous layer. Thereafter, the tape laminate was kept for drying for 48 h at ambient temperature.

Specimens of 3.2 cm diameter were punched from the dried bilayer green tape. For thermal processing of the bilayer specimens, two step procedure was adopted to achieve quality flat sintered specimens. First, they were subjected to binder burnout and partial sintering by initially heating up to 500 °C at the rate of 0.5 °C min^{-1} (binder burnout) and then to 1350 °C at the rate of 1 °C min^{-1} (partial sintering) and soaked at this temperature for 2 h. It was cooled down to room temperature at the rate of 2 °C min^{-1}. Secondly, it was further sintered by heating up to 1550 °C at the rate of 2 °C min^{-1} and thermally soaking at this temperature for 2 h before it was cooled down to room temperature at the rate of 2 °C min^{-1}. After the second sintering, all the specimens became flat and two layers (porous and dense) were adequately bonded and could be handled without delamination. The average diameter of the specimens after the final sintering was 2.54 cm.

Similarly, tape cast and high temperature processing were implemented to obtain the single layer dense YSZ and YSZ–Al_2O_3 (20 wt%) composite electrolyte membranes for electrochemical characterization. Specimens were of 200–300 μm thick and 1.268 cm in diameter.

2.2. AC impedance measurement for YSZ and YSZ–Al_2O_3 electrolyte membranes

Both sides of the YSZ and YSZ–Al_2O_3 composite electrolyte membranes were platinum coated and fired at 850 °C for 0.5 h. Each specimen was sandwiched between two symmetric stainless steel blocking electrodes and placed into a high temperature Macor® holder. The holder containing the SS/electrolyte/SS cell was subsequently placed into a high temperature furnace (RHF 1600 Carbolite, Hope Valley, S33 6RB, England). AC impedance in the 600–797 °C temperature range was carried out using Solartron impedance spectroscopy analyzer (Model 1260 with an electrochemical interface; Solartron US, Houston, TX) in the 0.01–100 kHz frequency range. *Z* plot and *Z* view softwares were employed for data acquisition and analysis. At each temperature, the specimen was equilibrated for 1 h before the impedance measurement.

2.3. Interlayer and cathode application

A paste of YSZ–Al_2O_3 (20 wt%) – lanthanum strontium manganate [LSM, NexTech Materials Ltd., Lewis Center, OH] in 1:1 proportion as an interlayer was first applied to the electrolyte side of the sintered YSZ–Al_2O_3 bilayer using a paint brush and dried in air. Subsequently, another layer of LSM-graphite (10 wt%) as cathode was applied on the dried interlayer. After drying it was sintered at 1200 °C for 2 h. The interlayer and cathodic pastes were prepared using ethanol–xylene (1:1) medium.

2.4. Anode preparation on the porous layer of the bilayer

The porous side (porosity ∼64.15%) of the YSZ–Al_2O_3 (20 wt%) composite bilayer was initially infiltrated with aqueous solution of cerium nitrate (Alfa Aesar, Ward Hill, MA) and calcined at 450 °C for 1 h. The infiltration process was repeated for few times. These infiltrations and calcinations introduced about 11.85 wt% of ceria (CeO_2) into the porous anode. The anodic side of the specimen became cream colored after CeO_2 infiltration and calcination. This specimen was further infiltrated with aqueous solution of copper nitrate and followed by a

calcination at 450 °C for an hour. This process was repeated for over a dozen times. After these infiltrations and calcinations, 30.67 wt% of CuO was deposited into the pores. The equivalent amount of metallic copper (Cu) for the infiltrated CuO is 24.16 wt%. The weight ratio of CeO_2 and Cu introduced in the specimen was approximately 1:2. This proportion was practiced as it was found that the conductivity with similar content of ceria and copper in the pores of YSZ was close to the maximum value [6]. This proportion was also adopted by Park et al. [7] in processing the anode in the 50% porous and dense YSZ bilayer.

2.5. Cell assembly and electrochemical measurements

A platinum paste (ESL ElectroScience, King of Prussia, PA) was applied onto the platinum lead (Alfa Aesar, Ward Hill, MA) in contact with the anodic side of the cell. It was then placed inside a high temperature furnace (RHF 1600 Carbolite, Hope Valley, S33 6RB, England) and the temperature was initially raised up to 400 °C at the rate of 0.5 °C min^{-1} and then increased to 980 °C at the rate of 1 °C min^{-1} and soaked at this temperature for about 0.33 h. Subsequently, it was cooled down to room temperature at the rate of 2 °C min^{-1}. Similar processing method was used for attaching the platinum lead to the cathode side of the cell. However, the lead was attached to the cathode side of the cell prior to the introduction of ceria and copper on the anode side of the cell.

The cell was sealed to an alumina tube [(outer diameter 2.54 cm & inner diameter 1.9 cm), AdValue Technology, Tucson, AZ] using the high temperature cement (Ceramabond 552, Aremco Products Inc., Valley Cottage, NY). Then the cell assembly was placed into a programmable furnace (F79300, Barnstead-Thermolyne Inc., Dubuque, IA) for testing at various temperatures.

The impedance measurement of the cell was measured in the 650–800 °C temperature range using the same impedance spectrometer (0.01–10^6 Hz frequency range). *Z* plot and *Z* view softwares were used for data acquisition and analysis.

The button cell was evaluated under hydrogen/air and propane/air atmospheres at these temperatures using a fuel cell test station, Solartron Analytical 1400 + 1470E (Solartron Analytical, Farnborough, Hampshire, UK). The propane fuel as supplied by the Western Outdoors Inc. (Portland, OR) was directly fed to the fuel cell during the test.

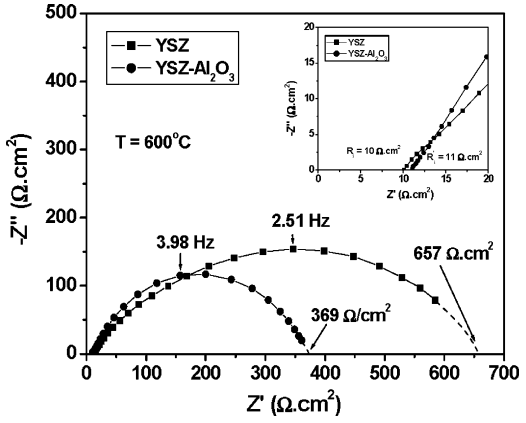

Fig. 1. Impedance spectra for YSZ and YSZ–Al_2O_3 (20 wt%) composite electrolyte membranes at 600 °C. Inset shows the blown up plot at the high frequency region.

2.6. Scanning electron microscopy

Scanning electron microscopy (SEM) investigations were conducted for the YSZ–Al_2O_3 cell using a high resolution scanning electron microscope (Hitachi S-4800 HRSEM; Hitachi High Technologies America Inc., Pleasanton, CA).

3. Results and discussion

3.1. Impedance and microstructure of YSZ–Al_2O_3 membranes

Typical impedance spectra of YSZ and YSZ–Al_2O_3 (20 wt%) membranes at 600 °C are shown in Fig. 1. Spectra consist of one major semi circle with seemingly another one at high frequency in both the YSZ and YSZ–Al_2O_3 membranes. The inset of Fig. 1 shows an enlarged view of the high frequency part of the segments, which exhibit existence of additional semicircle seemingly merged to the major semicircle originating from non-zero points of the Z' axis. The non-zero points for YSZ and YSZ–Al_2O_3 specimens which is interpreted as the circuit resistance external to the specimen are 10 and 11 Ω cm^2 respectively. The intersections (diameter) of the semicircles on the Z' axis are interpreted as the bulk area specific resistance of the membranes which are about 657 and 369 Ω cm^2 for YSZ and YSZ–Al_2O_3 membranes, respectively.

The YSZ–Al_2O_3 electrolyte exhibits more than two semicircles representing losses from YSZ grain, YSZ–YSZ grain boundary and YSZ–Al_2O_3 interfaces [5]. Although at higher temperatures (653–797 °C) the YSZ grain becomes very conductive and resulting impedance becomes negligible. Similarly, YSZ–Al_2O_3 interfaces are very conductive at higher temperatures and its impedance is less than the impedance of YSZ–YSZ grain boundary. Also the cumulative impedance of YSZ–YSZ grain boundary and YSZ–Al_2O_3 interfaces is less than the impedance of pure YSZ polycrystalline material at similar temperatures [5].

Fig. 2 shows the temperature dependence of the circuit resistance external to the specimen. An average area specific resistance of 10.55–1.77 Ω cm^2 in the 600–797 °C temperature range with a cross-over between the YSZ and YSZ–Al_2O_3 composite membrane resistances at around 670 °C is depicted. At the lower temperature (<670 °C), a strong temperature dependence is displayed whereas at the higher temperature (>670 °C) a weak temperature dependence is exhibited.

A relative comparison of Arrhenius plots of the bulk conductivities of YSZ and YSZ–Al_2O_3 electrolytes is shown in Fig. 3. It is apparent that YSZ–Al_2O_3 composite electrolyte possesses about four to six times higher conductivity as compared to the YSZ material in the temperature range of 650–800 °C. The enhanced conductivity of the YSZ–Al_2O_3 composite electrolyte has been attributed to the space charge for-

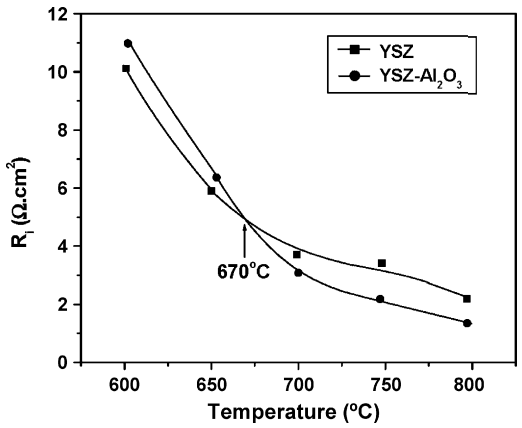

Fig. 2. Temperature dependence of the contact resistance of the YSZ and YSZ–Al_2O_3 (20 wt%) composite electrolyte membranes.

mation, which resulted from an interaction of Al_2O_3 and oxygen vacancies.

The conductivity data of Fig. 3 further suggests that the electrolyte thickness in the case of YSZ–Al_2O_3 composite can be increased by a factor of six at 800 °C as compared to the YSZ while maintaining similar power output. The superior conductive attribute of the composite electrolyte justified fabrication of thicker (50 μm) electrolyte cells in this investigation.

The presence of a dielectric phase, Al_2O_3 in YSZ matrix may lead to two antagonistic influences: (a) the blocking effect and (b) space charge effect. The blocking effect is characterized by a decline of ionic conductivity such as shown in Fig. 4. The space charge effect in certain situations can lead to an enhancement in conductivity, Fig. 4. Collectively, these two factors determine whether a given solid ionic conductor will have an enhancement in conductivity with the addition of a dielectric phase or not. The blocking and space charge effects can be delineated and quantified in different temperature regions, especially in simpler systems such as single lithium ion conductor doped with dielectric phases [8]. Such a delineation could not be carried out for the YSZ–Al_2O_3 system because of limited temperature

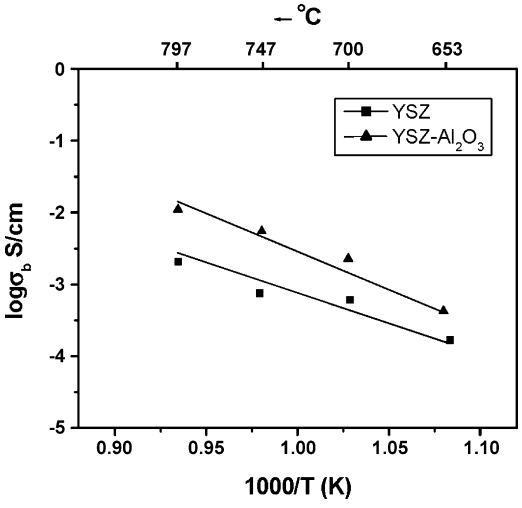

Fig. 3. Arrhenius plots of bulk conductivities shown as $\log \sigma_b$ vs. 1000/T for YSZ and YSZ–Al_2O_3 (20 wt%) composite electrolyte membranes.

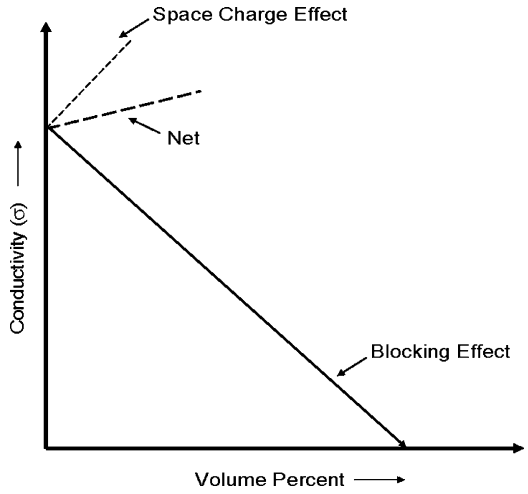

Fig. 4. Schematic representation of effect of Al_2O_3 dopant on conductivity of YSZ–Al_2O_3 specimen.

range of conductivity data. Nonetheless, it can be stated that the blocking and space charge effects co-exist in the YSZ–Al_2O_3 (20 wt%) specimen and the magnitude of the space charge effect is greater than the magnitude of the blocking effect which results in a net enhancement of conductivity as shown in Fig. 4.

The microstructure of YSZ–Al_2O_3 (20 wt%) membrane is shown in Fig. 5. The larger YSZ grains form distinct grain boundaries. The continuity of YSZ matrix is impeded by the existence of irregular, darker Al_2O_3 phase. The YSZ–YSZ grain boundaries can be described as linear forming triple points whereas the YSZ–Al_2O_3 interfaces can be characterized as non-linear, irregular forming a complex pattern of microstructure. The YSZ–Al_2O_3 interfaces are electrically active and associated with impedance even lower than the impedance of the YSZ–YSZ grain boundaries. The Fig. 5 also shows existence of isolated pores (≃250 nm in size). The membrane thickness used for fabricating cells for this paper is about 50 μm and therefore these pores are expected to closed rather than open.

3.2. Cell performance with hydrogen and propane fuels

The SOFC cell temperature was slowly raised to 600 °C under hydrogen atmosphere, which allowed CuO to be reduced to metallic copper *in situ*. Copper primarily provides electronic

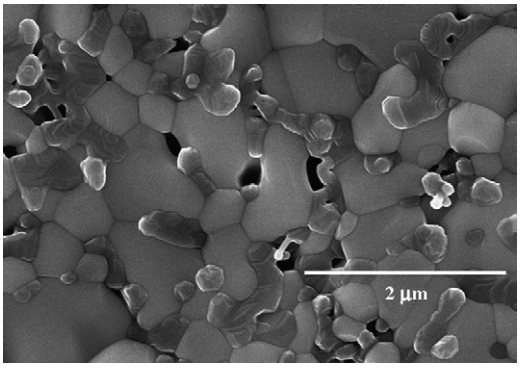

Fig. 5. Microstructure of the YSZ–Al_2O_3 (20 wt%) membrane.

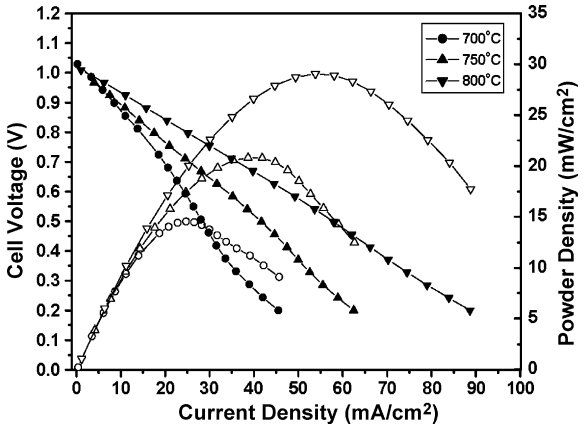

Fig. 6. Cell potential and power densities for Cu–CeO_2/YSZ–Al_2O_3/LSM cell operated with H_2 fuel at various temperatures.

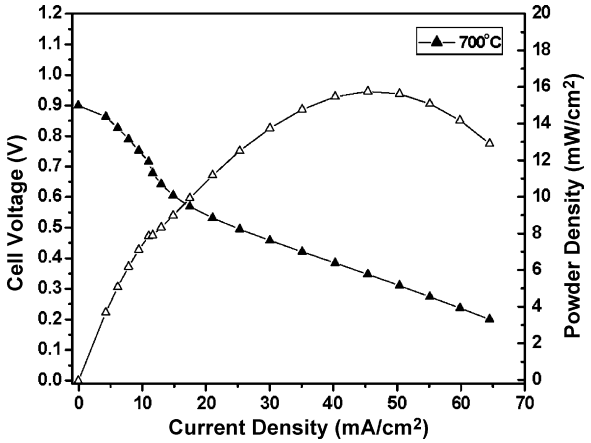

Fig. 7. Cell potential and power density for Cu–CeO_2/YSZ–Al_2O_3/LSM cell operated with propane fuel at 700 °C.

conduction. Furthermore, since it is a poor catalyst for hydrocarbon oxidation, it minimizes the formation of carbon, which is detrimental to the cell performance. The role of CeO_2 is very important [9,10] for the performance of SOFCs characterized in this investigation. The triple function of CeO_2, i.e., to act as oxidation catalyst, conduct oxygen ions and transport electrons in the anodic structure is well documented in the literature [11,12]. Also, specific functions of CeO_2 and Cu in the anode have been delineated by McIntosh [10].

Fig. 6 presents cell performance data (cell voltage, V and power density) as a function of current density (j) using hydrogen as the fuel. The j–V curves at lower temperatures (700 and 750 °C) show non-linearity – perhaps related to the conduction mechanism in the electrolyte. The mechanism involves formation and stability of the space charge effect. Instability of the formed space charge can be influenced by either temperature or electric field (here in context of high current density) or both. At 800 °C a linear j–V curve indicates a single Ohmic loss mechanism.

As expected, the power density increases with increasing temperature and reaches a peak value of about 29.03 mW cm^{-2} at 800 °C. Since the YSZ–Al_2O_3 composite electrolytes are intended for low temperature applications, electrochemical measurements were not conducted above 800 °C.

Fig. 7 shows the electrochemical performance data at 700 °C using propane as a fuel. The same cell was evaluated earlier using hydrogen as the fuel (Fig. 6). Under propane the OCV is reduced from 1.03 to 0.9 V. Such a reduction in OCV due to the use of hydrocarbon fuels has been reported earlier [9]. Furthermore, a steep decline in cell voltage at current densities less than 15 mA cm^{-2} relates to higher activation losses. At higher current densities (>15 mA cm^{-2}) the Ohmic loss dominates. The peak power density of 15.76 mW cm^{-2} is slightly greater than the peak power density (14.55 mW cm^{-2}) of the cell under hydrogen (Fig. 6). Inspite of the major activation loss, the performance of the cell is better in propane as compared to hydrogen.

Table 2 summarizes the cell performance with hydrogen and propane fuels. The small decrease in OCV and enhancement in power densities with increasing temperature are characteristics of SOFCs. The high OCV also suggest an absence of fuel leakage through the cell or the seal of the test fixture.

3.3. Cell impedance

Electrochemical impedance spectroscopy (EIS) was used to elucidate the loss mechanisms in the cell. The spectra were taken at open circuit voltage (OCV) and shown by the Nyquist plots in Fig. 8(A)–(D) respectively. The cell was evaluated utilizing hydrogen as a fuel at 650, 700, 750, and 800 °C. These plots show the existence of at least two semicircles or time constants which are associated with the occurrence of different electrochemical processes that may include electrode mass transfer, charge transfer kinetics, and ionic conduction. The first of the features of Fig. 8 is related to the high frequency intercepts of the Z' axis and it is believed to be related to contact resistance external to the cell, such as current collection, and cell area specific Ohmic resistances (ASOR), respectively. These resistance values are somewhat high and comparable to the contact resistances observed for the YSZ and YSZ–Al_2O_3 composite electrolyte membranes as shown in Fig. 2.

The total area specific resistance represented by the two semicircles of Fig. 8 is typical of SOFCs of other designs, which have been reported at the similar temperatures [13]. It is also important to note that the plots appear to show the existence of a tail at the low frequency regime possibly relating to diffusion limitations caused by inadequate electrode porosity.

Table 2
Typical SOFC performance using H_2 and propane as fuels

Temperature (°C)	H_2		Propane	
	OCV (V)	PD_{max} (mW cm^{-2})	OCV (V)	PD_{max} (mW cm^{-2})
650	1.07	1.05		
700	1.03	14.55	0.9	15.76
750	1.00	20.82		
800	1.05	29.03		

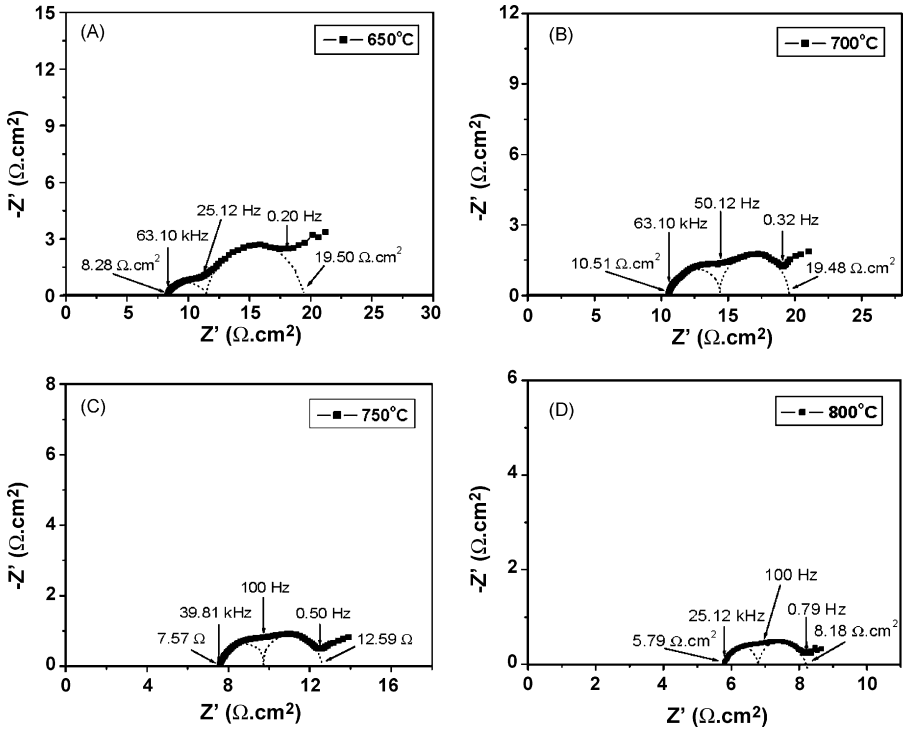

Fig. 8. Impedance spectra for Cu–CeO_2/YSZ–Al_2O_3/LSM cell at various temperatures.

3.4. Microstructure of cell components

Fig. 9 shows low resolution micrograph of the cell in which areas are marked (1), (2), (3), and (4). The area marked (1) represents the porous anode, which is about 450 μm thick and exhibits significant porosity that can accommodate and catalyze oxidation of fuels. The area marked (2) is the dense electrolyte comprising of YSZ–Al_2O_3 (20 wt%) and its thickness is about 50 μm. The [YSZ–Al_2O_3 (20 wt%)-LSM] interlayer is marked by area (3) and its thickness is about 20 μm. The cathode is about 180 μm thick and is labeled as (4). The cathode is highly porous and consists of only LSM. The total thickness of the cell is 700 μm.

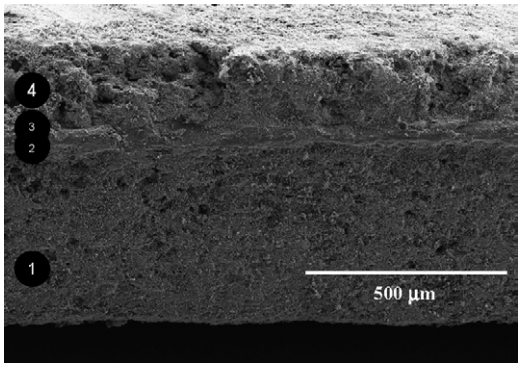

Fig. 9. SEM microstructure for Cu–CeO_2/YSZ–Al_2O_3/LSM cell showing the cross section view with index: (1) porous anode infiltrated with ceria and copper, (2) YSZ–Al_2O_3 (20 wt%) electrolyte, (3) YSZ–Al_2O_3 (20 wt%) LSM interlayer, and (4) LSM cathode.

Fig. 10(a)–(d) shows high resolution micrographs of each of the cell components. The anodic microstructure is shown in Fig. 10 (a) that depicts existence of large, copper aggregates – about 6 μm in diameter shown by an arrow in the micrograph. Small copper aggregates – about 0.5 μm in size are also shown in the micrograph. Existence of large and isolated copper aggregates in anode may play some role for the observed high Ohmic resistance of the cell [Fig. 8(A)–(D)]. The formation of large, isolated copper aggregates in similar SOFCs have been reported earlier [14].

The porosity of the anode layer was 64% prior to the inclusion of ceria and copper. The porosity was computed using the physical dimensions of the specimen. As visible from the Fig. 10(a), the porosity of the porous anode expectedly decreased to about 30% after the incorporation of 11.85 wt% CeO_2 and 24.16 wt% copper. The porosity of high performance anode is typically greater than 40%. This poor porosity of the anode after the infiltration of ceria and copper could be a factor for the observed low power density and the high Ohmic resistance for the cell. Such observations were reported by Lu et al. [15] in the SDC and ScSZ cells with low porosity of the LSGM anode.

The microstructure of the YSZ–Al_2O_3 (20 wt%) electrolyte layer is shown in Fig. 10(b), which is basically low resolution micrograph of Fig. 5. The dark areas of the Fig. 10 (b) depict the Al_2O_3 phase. The grain size of Al_2O_3, 0.5–1.7 μm, is smaller than the grain size of YSZ, 0.6–2.8 μm (particle size of the starting YSZ powder in the batch was 0.25 μm). During the high temperature processing, the Al_2O_3 particles have sintered into larger size grains as the particle size of Al_2O_3 as introduced in the batch was <47 nm. The doping of Al_2O_3 in the YSZ electrolyte impeded the YSZ growth and significant

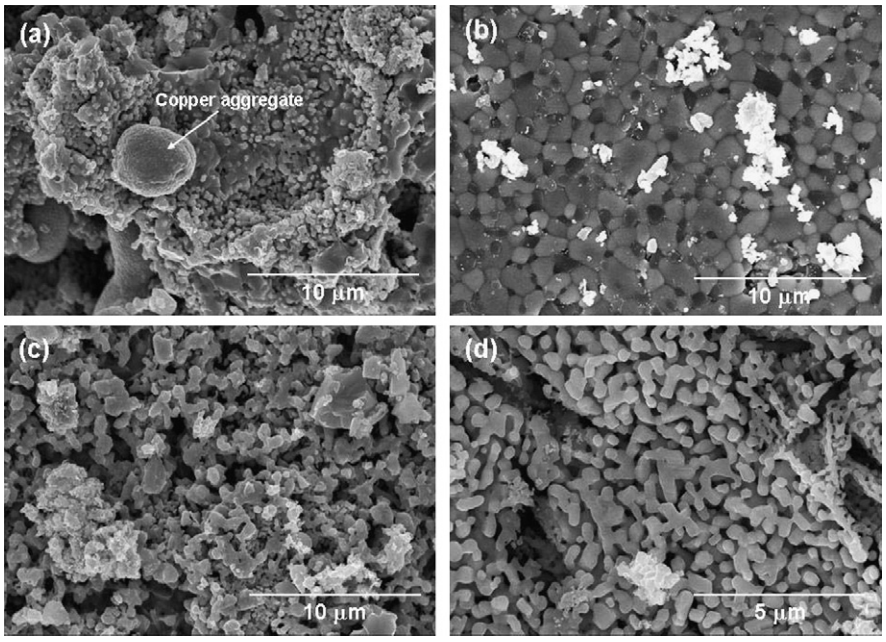

Fig. 10. SEM microstructures for each components of Cu-CeO_2/YSZ–Al_2O_3/LSM cell: (a) porous anode infiltrated with ceria and copper, (b) YSZ–Al_2O_3 (20 wt%) electrolyte, (c) YSZ–Al_2O_3 (20 wt%)-LSM interlayer, and (d) LSM cathode.

lattice strains were developed in both Al_2O_3 and YSZ grains. An evidence of the presence of structural defects by Al_2O_3 doping, formation of space charge regions, and space charge mediated ionic conductivity in YSZ–Al_2O_3 (20 wt%) electrolyte will be published elsewhere [5]. The desirable attributes of the YSZ–Al_2O_3 (20 wt%) electrolytes have allowed reasonable performance with 50 μm thick electrolyte at 700 and 800 °C.

A very thin (less than 20 μm) interlayer of [YSZ–Al_2O_3 (20 wt%)-LSM] was introduced in between the YSZ–Al_2O_3 (20 wt%) electrolyte and LSM cathode. This layer was incorporated to improve the charge transfer reaction between the electrolyte and cathode. An addition of the interlayer facilitated thermal expansion match between the electrolyte and cathode layers. The use of interlayer in the processing of SOFC is well documented in literature [16].

The microstructure of the YSZ–Al_2O_3 (20 wt%)-LSM interlayer in 1:1 proportion is shown in Fig. 10(c). A porous structure with LSM grains is evident in the microstructure. YSZ and Al_2O_3 grains are not prominently visible as their usual texture is modified by presence of LSM material.

Elongated morphology of LSM in the cathode is pronounced in Fig. 10(d). The aspect ratio of these elongated grains is about 5–7. Also, there is considerable amount of porosity as needed for an effective use of the oxidant.

4. Conclusions

A direct oxidation SOFC fabricated from the YSZ–Al_2O_3 composite electrolyte was evaluated using hydrogen and propane as fuels. The anodic structure comprised of CeO_2 and Cu contained in the porous YSZ–Al_2O_3 (20 wt%) composite layer. An interlayer consisting of YSZ–Al_2O_3 (20 wt%) composite electrolyte and LSM, and cathode consisting of LSM were employed. The rationale for the use of the composite electrolyte was based on its enhanced conductivity and low cost as compared to the YSZ. The OCV utilizing hydrogen fuel was in the range of 1.00–1.07 V close to the reversible thermodynamic potential. The peak power density at 800 °C with hydrogen was 29.03 $mWcm^{-2}$. Contrary to the expectation, the peak power density at 700 °C with propane was slightly higher than peak power density obtained with hydrogen.

Acknowledgements

Authors (JST and BK) gratefully acknowledge the financial support by the Air Force Research Laboratory, Propulsion Directorate, under contract No. FA 8650-04-D-2403, DO 05. The authors express sincere appreciation to Dr. Christina Chen for earlier processing of tape cast bilayers and Mr. Prashanth Nanganuri for preparing the direct oxidation anode.

References

[1] B. Kumar, C. Chen, C. Varanasi, J.P. Fellner, J. Power Sources 140 (2005) 12.
[2] C. Varanasi, C. Juneja, C. Chen, B. Kumar, J. Power Sources 147 (2005) 128.
[3] M. Mori, T. Abe, H. Itoh, O. Yamamoto, Y. Takeda, T. Kawahara, Solid State Ionics 74 (1994) 157.
[4] A.J. Feighery, J.T.S. Irvine, Solid State Ionics 121 (1999) 209–216.
[5] B. Kumar, J.S. Thokchom, J. Am. Ceram. Soc., in press.
[6] P. Nanganuri, Processing of anodes for SOFC, Master Thesis, Mechanical Engineering Department, University of Dayton (October, 2007).
[7] S. Park, R.J. Gorte, J.M. Vohs, J. Electrochem. Soc. 148 (2001) A443.
[8] B. Kumar, S. Nellutla, J.S. Thokchom, C. Chen, J. Power Sources 160 (2006) 1329.
[9] R.J. Gorte, H. Kim, J.M. Vohs, J. Power Sources 106 (2002) 10.
[10] S. McIntosh, J.M. Vohs, R.J. Gorte, Electrochim. Acta 47 (2002) 3815.

[11] C.R. Xia, M.L. Liu, Solid State Ionics 152–153 (2002) 423.
[12] Y. Matsuzaki, I. Yasuda, Solid State Ionics 152–153 (2002) 463.
[13] T.L. Reitz, H. Xiao, M. Rottmayer, T. Siebert, A longevity study of solid oxide fuel cells for intermediate temperature operation, ECS Trans. 7 (2007) 687.
[14] S. Jung, C. Lu, H. He, K. Ahn, R.J. Gorte, J.M. Vohs, J. Power Sources 154 (2006) 42.
[15] C. Lu, A. An, W.L. Worrel, J.M. Vohs, R.J. Gorte, Solid State Ionics 175 (2004) 47.
[16] T.L. Reitz, H. Xiao, J. Power Sources 161 (2006) 437.